

Formatted: Numbering: Continuous

# 1 Early winter barium excess in the Southern Indian Ocean as an 2 annual remineralisation proxy (GEOTRACES GIPr07 cruise)

3 Natasha René van Horsten<sup>1,2,3</sup>, H el ene Planquette<sup>1</sup>, G eraldine Sarthou<sup>1</sup>, Thomas James Ryan-Keogh<sup>2</sup>,  
4 Nolwenn Lemaitre<sup>5</sup>, Thato Nicholas Mtshali<sup>4</sup>, Alakendra Roychoudhury<sup>3</sup>, and Eva Bucciarelli<sup>1</sup>

5 <sup>1</sup>Univ Brest, CNRS, IRD, Ifremer, LEMAR, F-29280 Plouzane, France.

6 <sup>2</sup>SOCCO, CSIR, Lower Hope road, Cape Town, South Africa, 7700.

7 <sup>3</sup>TracEx, Department of Earth Sciences, Stellenbosch University, Stellenbosch, South Africa, 7600.

8 <sup>4</sup>Department of Forestry, Fisheries and Environment, Oceans and Coast, Foretrust Building, Martin Hammerslag Way, Cape  
9 Town, South Africa, 8001

10 <sup>5</sup>Department of Earth Sciences, Institute of Geochemistry and Petrology, ETH Zurich, Zurich, Switzerland.

11 *Correspondence to:* Natasha van Horsten (nvhorsten@csir.co.za), Eva Bucciarelli (Eva.Bucciarelli@univ-brest.fr)

Deleted: Environment,

Deleted: and

12 **Abstract.** The Southern Ocean (SO) is of global importance to the carbon cycle, and processes such as mesopelagic  
13 remineralisation that impact the efficiency of the biological carbon pump in this region need to be better constrained. During  
14 this study early austral winter barium excess ( $Ba_{xs}$ ) concentrations were measured for the first time, along 30 E in the Southern  
15 Indian Ocean. Winter  $Ba_{xs}$  concentrations of 59 to 684 pmol L<sup>-1</sup> were comparable to those observed throughout other seasons.  
16 The expected decline of the mesopelagic  $Ba_{xs}$  signal to background values during winter was not observed, supporting the  
17 hypothesis that this remineralisation proxy likely has a longer timescale than previously reported. A compilation of available  
18 SO mesopelagic  $Ba_{xs}$  data, including data from this study, shows an accumulation rate of  $\sim 0.9 \mu\text{mol m}^{-2} \text{d}^{-1}$  from September  
19 to July that correlates with temporally integrated remotely sensed primary productivity (PP), throughout the SO from data  
20 spanning  $\sim 20$  years, advocating for a possible annual timescale of this proxy. The percentage of mesopelagic POC  
21 remineralisation as calculated from estimated POC remineralisation fluxes over integrated remotely sensed PP was  $\sim 2$  fold  
22 higher south of the polar front ( $19 \pm 15 \%$ ,  $n = 39$ ) than north of the polar front ( $10 \pm 10 \%$ ,  $n = 29$ ), revealing the higher  
23 surface carbon export efficiency further south. By linking integrated remotely sensed PP to mesopelagic  $Ba_{xs}$  stock we could  
24 obtain better estimates of carbon export and remineralisation signals within the SO on annual and basin scales.

## 25 1 Introduction

26 The Southern Ocean (SO) is a carbon sink of global significance responsible for 40 – 50 % of the global oceans' carbon uptake  
27 (Friedlingstein et al., 2019; Gregor et al., 2019; Gruber et al., 2019). Oceanic carbon uptake is regulated by various processes,  
28 including the biological carbon pump (BCP). Inorganic carbon is consumed and released by photosynthetic organisms through  
29 photosynthesis and respiration (Sarmiento and Gruber, 2006), thereby regulating the earth's carbon cycle by partially

32 sequestering photosynthetically fixed CO<sub>2</sub> in the ocean interior (Honjo et al., 2014). In particular, the SO BCP is a crucial  
33 contributor to the earth's carbon cycle by exporting, from surface waters, ~ 3 Pg C yr<sup>-1</sup> of the ~ 10 Pg C yr<sup>-1</sup> global export  
34 production (Schlitzer, 2002). The efficiency of the BCP is linked to the export and preservation of surface particulate matter  
35 and is directly linked to atmospheric CO<sub>2</sub> levels, on glacial-interglacial timescales (Honjo et al., 2014; Sigman et al., 2010).  
36 Sedimentation out of the surface layer (~100 m) is defined as surface export and out of the mesopelagic zone (~1000 m) as  
37 deep export (Passow and Carlow, 2012). There are large gaps in our knowledge with regard to deep carbon export, internal  
38 cycling and the seasonality of these processes (Takahashi et al., 2012). The magnitude of deep carbon export is dependent on  
39 the efficiency of mesopelagic remineralisation (Jacquet et al., 2015) which can balance or even exceed particulate organic  
40 carbon (POC) surface export, especially later in the growing season, thereby limiting deep export (Buesseler and Boyd, 2009;  
41 Cardinal et al., 2005; Jacquet et al., 2011, 2015; Lemaitre et al., 2018; Planchon et al., 2013). A possible explanation for  
42 imbalances between surface export and mesopelagic processes can be lateral advection of surface waters with lower particle  
43 export relative to the mesopelagic signal (Planchon et al., 2013). It is also possible that continued remineralisation of earlier  
44 larger export fluxes is detected in the mesopelagic signal but not in the export fluxes of in situ observations (Planchon et al.,  
45 2013). In addition to this, the efficiency of remineralisation is influenced by the size and composition of exported particles  
46 (Rosengard et al., 2015; Twining et al., 2014) as well as the pathway by which these particles are transported downwards (e.g.,  
47 eddy-subduction, active migration, sinking or mixing) from the surface mixed layer to the mesopelagic zone (Boyd et al., 2019;  
48 Le Moigne, 2019), creating an intricate web of processes to disentangle. Mesopelagic remineralisation has also been shown to  
49 be influenced by environmental factors, such as temperature, phytoplankton community structure and nutrient availability  
50 (Bopp et al., 2013; Buesseler and Boyd, 2009). Indeed, nutrient limitation in surface waters limits export and consequently  
51 mesopelagic remineralisation by promoting the shift to smaller phytoplankton assemblages that preferentially take up recycled  
52 nutrients in the surface mixed layer (Planchon et al., 2013). Phytoplankton community composition exerts an important control  
53 where diatoms are more efficiently exported, due to their large size and ballasting by biogenic silica, compared to smaller non-  
54 diatom phytoplankton (Armstrong et al., 2009; Buesseler, 1998; Ducklow et al., 2001). Latitudinal trends in remineralisation  
55 efficiency can also be linked to temperature-dependent heterotrophs that are responsible for remineralisation (DeVries and  
56 Weber, 2017; Marsay et al., 2015). The mesopelagic layer is under-studied, especially in the high latitudes, and therefore these  
57 processes are poorly constrained, despite their importance to global elemental cycles, including that of carbon (Le Moigne,  
58 2019; Robinson et al., 2010).

59 Export and remineralisation tracers, such as <sup>234</sup>Th/<sup>238</sup>U and apparent oxygen utilization (AOU), have been used to study  
60 mesopelagic POC remineralisation fluxes (Buesseler et al., 2005; Planchon et al., 2013; Lemaitre et al., 2018). Surface export  
61 is set by the deficit of <sup>234</sup>Th activities over <sup>238</sup>U activities, while remineralisation processes are reflected by <sup>234</sup>Th/<sup>238</sup>U ratios  
62 larger than 1 below the surface mixed layer integrating processes over a 2 to 3 week period (Buesseler et al., 2005; Planchon  
63 et al., 2013). AOU is the depletion of oxygen (O<sub>2</sub>) in the ocean interior relative to surface saturation, due to biological  
64 respiration, when surface water masses are subducted. AOU is dependent on salinity and temperature and integrates  
65 remineralisation on timescales of years to decades (Ito et al., 2004). Inaccuracies have, however, been detected with AOU as

66 a remineralisation proxy, specifically in high latitude areas, due to O<sub>2</sub> undersaturation as a consequence of large temperature  
67 gradients (Ito et al., 2004).

68 Barium excess (Ba<sub>xs</sub>) is another proxy utilised to yield estimates of mesopelagic POC remineralisation fluxes. It is defined as  
69 the “biogenic” portion of particulate barium (pBa) as barite crystals, formed by the decay of bio-aggregates below the surface  
70 mixed layer (Bishop, 1988; Dehairs et al., 1980; Lam and Bishop, 2007; Legeleux and Reyss, 1996; van Beek et al., 2007). As  
71 these crystals are released, a Ba<sub>xs</sub> peak is formed within the mesopelagic zone which has been found to correlate to primary  
72 production (PP), O<sub>2</sub> consumption and POC remineralisation (Dehairs and Goeyens, 1996; Dehairs et al., 1997). Depth-  
73 integrated rates of O<sub>2</sub> consumption between the base of the mixed layer and 1000 m were estimated using an inverse 1-D  
74 advection-diffusion-consumption model (Shopova et al., 1995) to develop transfer functions between the Ba<sub>xs</sub> signal and the  
75 rate of surface POC export for subsequent mesopelagic remineralisation (Dehairs and Goeyens, 1996; Dehairs et al., 1997).  
76 Strong correlations have been obtained between the well-established export/remineralisation flux proxy <sup>234</sup>Th and Ba<sub>xs</sub>, during  
77 studies conducted in the SO and the North Atlantic, confirming the validity of Ba<sub>xs</sub> as a remineralisation proxy (Cardinal et  
78 al., 2005; Lemaitre et al., 2018; Planchon et al., 2013). Estimates of POC remineralisation fluxes, using the Ba<sub>xs</sub> proxy, are  
79 directly influenced by the background signal of Ba<sub>xs</sub>, after partial dissolution and sedimentation from the previous bloom  
80 season. It can be thought of as “pre-formed Ba<sub>xs</sub>”, defined as the Ba<sub>residual</sub> signal at zero O<sub>2</sub> consumption (Jacquet et al., 2015).  
81 Because studies conducted in spring and summer suggest that the mesopelagic Ba<sub>xs</sub> signal lasts between a few days to a few  
82 weeks (Dehairs et al., 1997; Cardinal et al., 2005; Jacquet et al., 2007, 2008a), it is postulated that winter measurements should  
83 give the true SO Ba<sub>residual</sub> value (Jacquet et al., 2008b, 2011). In this context, as part of a GEOTRACES process study (GIpr07)  
84 of a transect along 30°E in the Southern Indian Ocean (58.5°S to 41.0°S), we studied Ba<sub>xs</sub> distributions during early austral  
85 winter (July 2017) to better constrain the SO Ba<sub>residual</sub> concentrations and the timescale of this proxy. To our knowledge these  
86 are the first reported wintertime values for this proxy in the SO.

Deleted: utilized

Deleted: a

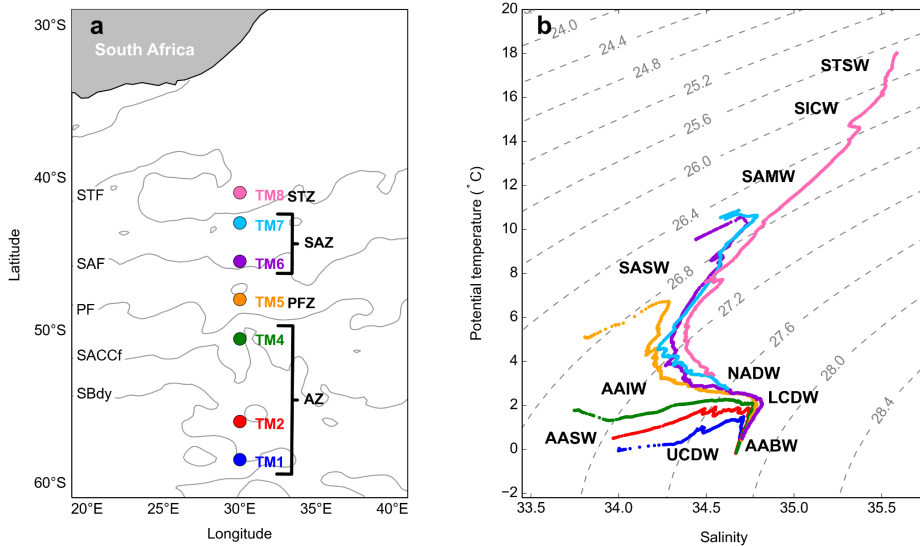
## 87 2 Materials and Methods

### 88 2.1 Sampling and hydrography

89 During the GEOTRACES GIpr07 cruise, which took place in early austral winter (28 June - 13 July 2017) onboard the R/V  
90 SA Agulhas II, seven stations were sampled along 30°E, from 58.5°S to 41.0°S (WOCE I06S, Figure 1a). At each station  
91 between 15 and 21 samples were collected from 25 m down to 1500 m, for shallow stations, and down to 4250 m, for deep  
92 stations, to be analysed for multiple parameters.

93 Positions of the fronts during the cruise were determined using the July monthly mean absolute dynamic topography data from  
94 the CLS/AVISO product (Rio et al., 2011), with boundary definitions from Swart et al. (2010). From north to south the  
95 identified fronts are, the Subtropical Front (STF), the Subantarctic Front (SAF), the Polar Front (PF), the Southern Antarctic  
96 Circumpolar Current Front (SACCF) and the Southern Boundary (SBdy) (Figure 1a). The marginal ice zone, identified as the

99 position of 30 % ice cover, was positioned at 61.7°S, approximately 3° (356 km) south of the southernmost station (de Jong et  
 00 al., 2018). Therefore, a potential sea ice influence on our study area can be disregarded.



01 **Figure 1:** (a) GEOTRACES GIPr07 cruise sampling stations overlaid on a map with frontal positions; namely, the Subtropical Front  
 02 (STF), the Subantarctic Front (SAF), the Polar Front (PF), the Southern Antarctic Circumpolar Current Front (SACCf) and the  
 03 Southern Boundary (SBdy), as determined by mean absolute dynamic topography (MADT) and crossing over four zones; namely,  
 04 the Antarctic zone (AZ), the Polar frontal zone (PFZ), the Subantarctic zone (SAZ) and the Subtropical zone (STZ). (b) Potential  
 05 temperature plotted against salinity, overlaid on isopycnals and identification of water masses sampled; namely, Subtropical Surface  
 06 Water (STSW), South Indian Central Water (SICW), Subantarctic Mode Water (SAMW), Subantarctic Surface Water (SASW),  
 07 Antarctic Intermediate Water (AAIW), Antarctic Surface Water (AASW), North Atlantic Deep Water (NADW), Lower  
 08 Circumpolar Deep Water (LCDW), Upper Circumpolar Deep Water (UCDW), and Antarctic Bottom Water (AABW).

## 10 2.2 Temperature, salinity and dissolved O<sub>2</sub>

11 Temperature (°C), salinity and dissolved O<sub>2</sub> (μmol L<sup>-1</sup>) profiles were measured by sensors (SBE 911plus) which were  
 12 calibrated by the manufacturer within a year prior to the cruise. At each cast, discrete seawater samples were collected and  
 13 analysed onboard for in situ calibration of sensor data for salinity (8410A Portasal salinometer, R<sup>2</sup> = 0.99) and dissolved O<sub>2</sub>  
 14 concentrations (Metrohm 848 titrimo plus, R<sup>2</sup> = 0.83; Ehrhardt et al., 1983). Temperature and salinity measurements were used  
 15 to calculate potential density (σ<sub>θ</sub>; Gill, 1982) to characterise water masses sampled and to identify the mixed layer depth  
 16 (MLD). The MLD is the depth at which there is a change of 0.03 kg m<sup>-3</sup> in σ<sub>θ</sub> from a near-surface value at ~ 10 m (de Boyer  
 17 Montégut, et al., 2004). Decreases in dissolved O<sub>2</sub> concentrations at intermediate depths, together with B<sub>axs</sub> concentrations,  
 18 were used to define the mesopelagic remineralisation layer.

### 19 2.3 pBa and pAl

20 Profile sampling of the water column was conducted with a GEOTRACES compliant trace metal clean CTD housed on an  
21 epoxy coated aluminium frame with titanium bolts equipped with 24 x 12 L trace metal clean Teflon coated GO-FLO bottles  
22 (General Oceanics). All sampling and analyses were conducted following the GEOTRACES clean sampling and analysis  
23 protocols (Cutter et al., 2017). Volumes of 2 to 7 L seawater were filtered from the GO-FLO bottles onto acid-washed  
24 polyethersulfone filters (25 mm diameter, Supor, 0.45  $\mu\text{m}$  pore size), for pBa and pAl analyses. Filters were mounted in-line  
25 on the side spigot of each Go-Flo bottle, on swinnex filter holders. Furthermore, bottles were mixed 3 times before filtration,  
26 as recommended by the GEOTRACES protocols (Cutter et al., 2017), to ensure homogenous sampling. Although the large  
27 fast-sinking fraction of particles may be undersampled by using bottles (Bishop and Edmond, 1976; Planquette and Sherrell,  
28 2012), comparing data that were generated using the same, internationally validated sampling systems and protocols (Cutter  
29 et al. 2017), as we do in this study, minimises potential bias. After filtration, filters were placed in trace metal clean petri slides  
30 (Pall) and kept frozen at  $-20^{\circ}\text{C}$  until further processing on land. Sample processing was conducted under a class 100 HEPA  
31 filtered laminar flow and extraction hood in a clean laboratory.

32 The pBa and pAl samples were processed and analysed 6 months after sample collection, at LEMAR (France). Unused blank  
33 filters and filters containing the samples were acid reflux digested at  $130^{\circ}\text{C}$  in acid-cleaned savillex vials using a mixture of  
34 HF and  $\text{HNO}_3$  (both Ultrapure grade, Merck) solutions (Planquette and Sherrell, 2012). Archive solutions were stored in 3 ml  
35 of 0.12 M  $\text{HNO}_3$  (Ultrapur grade), of which 250  $\mu\text{L}$  was diluted up to 2 mL for analysis by sector field inductively coupled  
36 plasma mass spectrometry (SF-ICP-MS, Element XR Thermo Scientific). Samples were spiked with  $1 \mu\text{g L}^{-1}$  indium as an  
37 internal standard to correct for instrument drift. The detection limits, defined as three times the standard deviation of the blanks  
38 (unused filter blanks), were  $0.39 \text{ pmol L}^{-1}$  and  $0.03 \text{ nmol L}^{-1}$  ( $n = 5$ ) for pBa and pAl, respectively. Mean amounts (in nmol)  
39 of a given element determined in unused filter blanks were subtracted from the amounts in the sample filter then divided by  
40 the volume filtered. Three certified reference materials (BCR 414, MESS 4 and PACS 3) were processed and analysed with  
41 the samples to assess the accuracy of the methodology. Our values were in good agreement with the certified values of the  
42 reference materials (Table 1) (Jochum et al., 2005). Percentage error of analyses was determined by the repeat analysis of  
43 random samples during each run, the mean percentage error of sample analysis for pBa and pAl was  $9.2 \pm 2.5 \%$  and  $11.1 \pm$   
44  $4.6 \%$  (mean  $\pm$  SD,  $n = 6$ ), respectively.

45 **Table 1: Certified Reference Material recovery data for accuracy determination of pBa and pAl analyses**  
46 **N/A refers to instances where there are no certified values available to check for accuracy**

	pBa (mg/kg)	pAl (mg/kg)
PACS 3 certified (mean $\pm$ SD)	N/A	$65800 \pm 1700$
PACS 3 measured (mean $\pm$ SD)	N/A	$73156 \pm 15416$
PACS 3 mean % recovery	N/A	$111 \pm 23$

MESS 4 certified	920	79000 ± 2000
MESS 4 (mean ± SD)	1033 ± 28	100048 ± 26870
MESS 4 mean % recovery ± SD	112 ± 3	127 ± 34
BCR 414 indicative values	32 ± 5	2384 ± 652
BCR 414 (mean ± SD)	34 ± 4	2651 ± 317
BCR 414 mean % recovery ± SD	105 ± 12	111 ± 13

47

#### 48 2.4 Ba<sub>xs</sub> as a proxy for mesopelagic POC remineralisation

49 The non-lithogenic fraction of pBa, Ba<sub>xs</sub>, was calculated by subtracting the lithogenic fraction of pBa from the total pBa  
 50 measured using Eq. 1. The lithogenic contribution to pBa was calculated by multiplying the pAl concentration with the Ba/Al  
 51 upper continental crust (UCC) ratio, 0.00135, as determined by Taylor and McLennan (1985).

52

$$53 Ba_{xs} = [pBa] - ([pAl] \times (Ba/Al)_{UCC}) \quad (1)$$

54

55 Total pBa and Ba<sub>xs</sub> profiles were nearly identical with a mean percentage Ba<sub>xs</sub> to total pBa of 99 ± 1 % (mean ± SD, n = 124;  
 56 Table S2), indicating that pBa from lithogenic sources was negligible. This ensures the accurate estimation of Ba<sub>xs</sub>, which  
 57 requires that less than 50 % of pBa should be associated with lithogenic inputs (Dymond et al., 1992).

58 The mesopelagic POC remineralisation flux was estimated using Eq. 2 (Dehairs and Goeyens, 1996; Shopova et al., 1995);

59

$$60 Mesopelagic\ POC\ remineralisation = Z \times JO_2 \times (C:O_2)_{Redfield\ Ratio} \times 12.01 \quad (2)$$

61

62 Where the mesopelagic POC remineralisation flux is expressed in mg C m<sup>-2</sup> d<sup>-1</sup>, Z is the depth range of the mesopelagic Ba<sub>xs</sub>  
 63 layer (100 - 1000 m), C:O<sub>2</sub> is the stoichiometric molar ratio of carbon to O<sub>2</sub> consumption by remineralisation as per the Redfield  
 64 Ratio (127/175, Broecker et al., 1985), 12.01 is the molar mass of carbon (g mol<sup>-1</sup>) and JO<sub>2</sub> is the rate of O<sub>2</sub> consumption (μmol  
 65 L<sup>-1</sup> d<sup>-1</sup>) as estimated using Eq. 3.

66

$$67 JO_2 = (Mesopelagic\ Ba_{xs} - Ba_{residual})/17200 \quad (3)$$

68 Eq. 3 (Dehairs and Goeyens, 1996; Shopova et al., 1995) is the linearisation of the exponential function by Dehairs et al.  
 69 (1997). Mesopelagic Ba<sub>xs</sub> is the depth-weighted average Ba<sub>xs</sub> of the mesopelagic zone (pmol L<sup>-1</sup>), the constant value of 17200  
 70 is the slope of the linear regression of depth-weighted average Ba<sub>xs</sub> (pmol L<sup>-1</sup>) versus O<sub>2</sub> consumption rate (μmol L<sup>-1</sup> d<sup>-1</sup>) and

Deleted: et al., 1997

Deleted: , the linearisation of the exponential function by Dehairs et al. (1997), using data from the Indian and Atlantic sectors of the SO, and has since been used and validated by studies within the SO (Cardinal et al., 2005; Planchon et al., 2013).

Deleted: .

Deleted: Equation 2 results from the linearisation of the exponential function by Dehairs et al. (1997), both of which give similar results.

Deleted: ¶

Deleted: (Dehairs et al., 1996 and Goeyens, 1996; Shopova et al., 1995)...

Deleted:

Deleted: ¶

Where

Deleted: m

Deleted: using the Southern Ocean transfer function by Dehairs et al. (1997)

91  $B_{\text{residual}}$  is the deep ocean background value of  $B_{\text{a,ss}}$  at zero oxygen consumption. The literature value of  $180 \text{ pmol L}^{-1}$  was  
92 used as the  $B_{\text{residual}}$  value (Jacquet et al., 2008a; 2008b; 2011; 2015; Planchon et al., 2013) in our calculations.

93 The integrated mesopelagic  $B_{\text{a,ss}}$  stock ( $\mu\text{mol m}^{-2}$ ) over the mesopelagic layer (100 - 1000 m) was calculated from the depth-  
94 weighted average  $B_{\text{a,ss}}$  in order to investigate the link between the accumulated mesopelagic signal and the corresponding  
95 integrated remotely sensed primary productivity (PP).

## 96 2.5 Integrated remotely sensed PP

97 The integrated remotely sensed PP ( $\text{mg C m}^{-2} \text{ d}^{-1}$ ) within the surface mixed layer was calculated using the CbPM algorithm  
98 (Behrenfeld et al., 2005), which requires chlorophyll concentration ( $\text{mg m}^{-3}$ ), particulate backscatter ( $\lambda 443 \text{ nm, m}^{-1}$ ),  
99 photosynthetically active radiation (PAR;  $\mu\text{mol photons m}^{-2} \text{ d}^{-1}$ ) and the MLD (m). Ocean Colour-Climate Change Initiative  
:00 (OC-CCI) data (<https://esa-oceancolour-cci.org/>), which blends existing data streams into a coherent record, meeting the  
:01 quality requirements for climate assessment (Sathyendranath et al., 2019), were used for chlorophyll and particulate  
:02 backscatter. PAR was taken from GLOB colour (<http://www.globcolour.info/>), and the MLD was taken from the climatology  
:03 of de Boyer Montegut et al. (2004). The integrated remotely sensed PP data were regridded to  $0.25^\circ$  spatially, using bilinear  
:04 interpolation using the Python programming package xESMF (Zhuang, 2018), and averaged monthly. The area-averaged PP  
:05 was averaged over a  $6 \times 1^\circ$  rectangular sample area, positioned  $6^\circ$  upstream longitudinally, and  $1^\circ$  latitudinally centred around  
:06 each sampled station (see discussion for details). In order to assess the validity of the remotely sensed PP data and demonstrate  
:07 no meridional bias across the SO, the percentage valid pixels was calculated for data north ( $90 \pm 20 \%$ ; mean  $\pm$  SD,  $n = 370$ )  
:08 and south ( $82 \pm 29 \%$  mean  $\pm$  SD,  $n = 488$ ) of the PF, revealing no bias.

## :09 2.6 Integrated % POC remineralised

:10 The integrated remineralised POC ( $\text{mg C m}^{-2}$ ) was estimated by multiplying the POC remineralisation flux ( $\text{mg C m}^{-2} \text{ d}^{-1}$ ), as  
:11 estimated using the  $B_{\text{a,ss}}$  proxy method, by the number of days over which the corresponding remotely sensed PP ( $\text{mg C m}^{-2} \text{ d}^{-1}$ )  
:12 was subsampled. The % POC remineralised was then estimated as the percentage of integrated remotely sensed PP ( $\text{mg C}$   
:13  $\text{m}^{-2}$ ) remineralised, assuming that the mesopelagic  $B_{\text{a,ss}}$  stock signal observed is due to the remineralisation of the integrated  
:14 surface PP signal.

## :15 2.7 Statistical analysis

:16 For statistical analysis, the least squares regression method was applied for assessment of significant correlations (Barbur et  
:17 al., 1994). Significant differences between regions and regressions were tested using Welch's t-test, with an alpha of 0.05 (95  
:18 % confidence level) (Kokoska and Zwillinger, 2000).

Deleted: Dehairs et al., 1997

## 20 3 Results

### 21 3.1 Hydrography

22 The potential temperature ( $\theta$ ) and salinity (S) along the transect ranged from -0.06 to 18.03 °C and from 33.77 to 35.59,  
23 respectively. Where surface  $\theta$  and S define four hydrographic zones; namely, the Antarctic zone (AZ;  $\theta < 2.5$  °C;  $S \leq 34$ ) from  
24 ~ 50°S to 58.5°S, the polar frontal zone (PFZ;  $\theta \cong 5$  °C;  $S \cong 33.8$ ) at ~ 48°S, the subantarctic zone (SAZ;  $5 < \theta < 11$  °C;  $33.8$   
25  $< S < 34.7$ ) between 43°S and 45.5°S, and the subtropical zone (STZ;  $\theta \geq 17.9$  °C;  $S \cong 35.6$ ) at 41°S (Figure 1a; Anilkumar  
26 and Sabu, 2017; Orsi et al., 1995; Pollard et al., 2002). The MLDs along the transect ranged between 97 and 215 m ( $144 \pm 39$   
27 m; mean  $\pm$  SD, n = 7), shoaling towards the PF (Table S1).

28 As can be observed on the T-S plot of stations sampled (Figure 1b), different water masses were sampled along the transect  
29 throughout the water column. South of the polar front (SPF;  $\cong 50^\circ\text{S}$ ; TM1, 2 and 4), from surface to depth, Antarctic Surface  
30 Water (AASW;  $27 < \sigma_\theta < 27.4$  kg.m<sup>-3</sup>), Upper and Lower Circumpolar Deep Water (UCDW;  $27.2 < \sigma_\theta < 27.75$  kg.m<sup>-3</sup> and  
31 LCDW;  $27.75 < \sigma_\theta < 27.85$  kg.m<sup>-3</sup>, respectively), and Antarctic Bottom Water (AABW;  $27.8 < \sigma_\theta < 27.85$  kg.m<sup>-3</sup>) were  
32 characterised. North of the polar front (NPF) and south of the STF ( $< 50^\circ\text{S}$ ; TM5, 6 and 7), from surface to depth, Subantarctic  
33 Surface Water (SASW;  $26.5 < \sigma_\theta < 26.75$  kg.m<sup>-3</sup>), Antarctic Intermediate Water (AAIW;  $26.7 < \sigma_\theta < 27.4$  kg.m<sup>-3</sup>), North  
34 Atlantic Deep Water (NADW;  $27 < \sigma_\theta < 27.85$  kg.m<sup>-3</sup>) and, as far north as 45.5°S, AABW close to the ocean floor, were  
35 identified. At the northernmost station (TM8; 41°S), in the STZ, the water masses sampled include Subtropical Surface Water  
36 (STSW;  $\sigma_\theta \cong 25.7$  kg.m<sup>-3</sup>), South Indian Central Water (SICW;  $25.8 < \sigma_\theta < 26.2$  kg.m<sup>-3</sup>), Subantarctic Mode Water (SAMW;  
37  $26.2 < \sigma_\theta < 26.6$  kg.m<sup>-3</sup>), AAIW and NADW.

### 38 3.2 Dissolved O<sub>2</sub>

39 The water column dissolved O<sub>2</sub> concentrations ranged from 159 to 333  $\mu\text{mol L}^{-1}$  (Figure 2). Maximum concentrations were  
40 observed in the surface mixed layer, increasing southwards along the transect, with a mean value of  $287 \pm 40$   $\mu\text{mol L}^{-1}$  (mean  
41  $\pm$  SD, n = 700). A decrease in concentrations below the MLD coincided with an increase in  $\sigma_\theta$ . South of the PF, the decrease  
42 in dissolved O<sub>2</sub> concentrations at the MLD was sharp and relatively shallow when compared to profiles NPF, which were more  
43 gradual, spanning a wider depth range. Within the mesopelagic zone concentrations decreased down to  $204 \pm 29$   $\mu\text{mol L}^{-1}$   
44 (mean  $\pm$  SD, n = 6373), then remained relatively uniform below 1000 m at  $192 \pm 113$   $\mu\text{mol L}^{-1}$  (mean  $\pm$  SD, n = 12950).

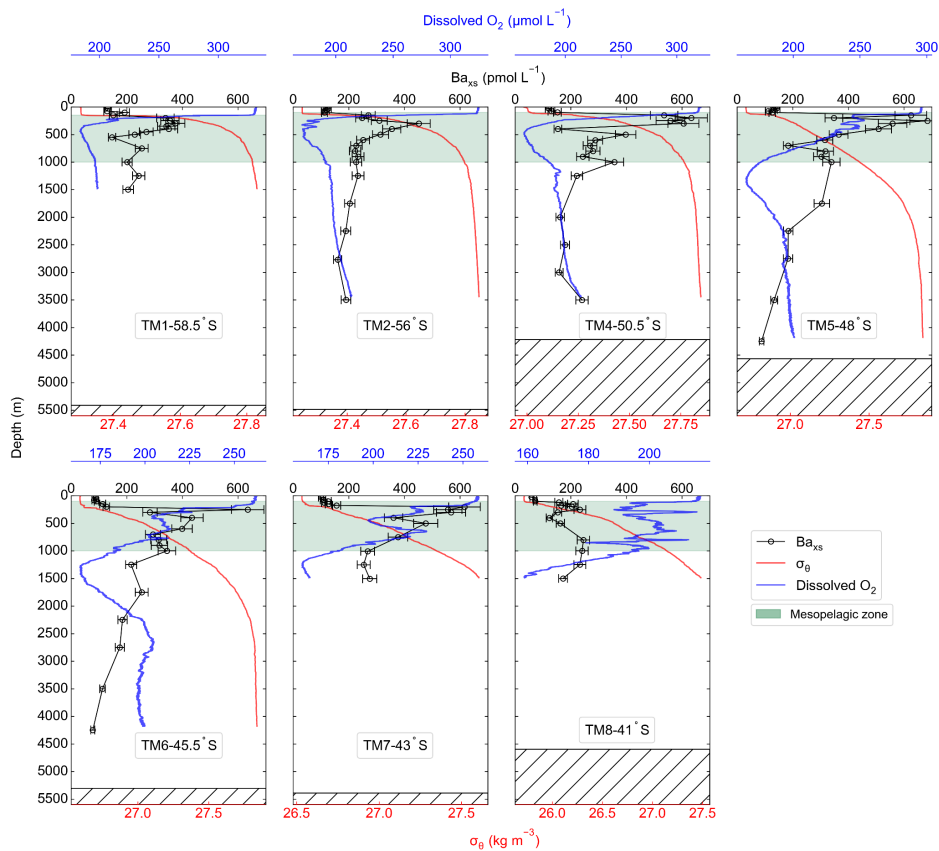


Figure 2:  $Ba_{xs}$  (black circles) with error bars, potential density ( $\sigma_{\theta}$ ; red) and dissolved  $O_2$  (blue) profiles sampled along the transect, plotted against depth, for stations TM1 to TM8, from south to north. The green shaded area is the mesopelagic zone, and the hatched area is the ocean floor.

### 3.3 $Ba_{xs}$ and estimated POC remineralisation fluxes

Along the transect,  $Ba_{xs}$  concentrations ranged from 59 to 684  $\text{pmol L}^{-1}$ . All profiles exhibited a depletion of  $Ba_{xs}$  in the upper surface waters (59 - 152  $\text{pmol L}^{-1}$ ), then a rapid increase below the MLD (~150 m), with concentrations ranging between 113 and 684  $\text{pmol L}^{-1}$  in the mesopelagic zone (100 - 1000 m, Figure 2). At the two southernmost stations (TM1 and TM2),

53 mesopelagic  $Ba_{\text{xs}}$  peaks spanned a narrower depth range (100 - 600 m) than stations further north, with concentrations reaching  
54 values of  $\sim 400 \text{ pmol L}^{-1}$ . Concentrations were higher in the PFZ and SAZ with a maximum of  $684 \text{ pmol L}^{-1}$  in the PFZ, at  
55  $48^\circ\text{S}$  (TM5). The subsurface increase of  $Ba_{\text{xs}}$  started at slightly deeper depths (150 - 200 m) and spanned wider depth ranges  
56 down to 1000 m, at stations north of the PF. The STZ station, at  $41^\circ\text{S}$  (TM8), had the lowest concentrations, only increasing  
57 up to  $\sim 200 \text{ pmol L}^{-1}$ . Double peaks were observed at all stations north of the PF, with a shallow and more substantial peak  
58 occurring in the upper mesopelagic zone and a second peak in the lower mesopelagic zone. Below the mesopelagic zone,  $Ba_{\text{xs}}$   
59 concentrations decreased down to  $\sim 180 \text{ pmol L}^{-1}$  and remained relatively uniform.

60 The mean  $Ba_{\text{residual}}$  concentration south of PF was  $183 \pm 29 \text{ pmol L}^{-1}$  (mean  $\pm$  SD,  $n = 7$ ), whereas it was  $142 \pm 45 \text{ pmol L}^{-1}$   
61 (mean  $\pm$  SD,  $n = 8$ ) between the PF and the STF. The two regions were however not significantly different to each other when  
62 conducting a Welch's t-test (t-statistic = 2.10; p-value = 0.06) and when averaging all concentrations below 2000 m along the  
63 transect, the  $Ba_{\text{residual}}$  concentration was  $161 \pm 43 \text{ pmol L}^{-1}$  (mean  $\pm$  SD,  $n = 15$ ). This concentration is not statistically different  
64 from the literature value of  $180 \text{ pmol L}^{-1}$  (Jacquet et al., 2008a; 2008b; 2011; 2015; Planchon et al., 2013), which is widely  
65 used for estimates of POC remineralisation fluxes. For a better comparison with these previous estimates, we used  $180 \text{ pmol}$   
66  $\text{L}^{-1}$  for the  $Ba_{\text{residual}}$  concentration in our calculations.

67 The estimated POC remineralisation fluxes for the study area ranged from 6 to  $96 \text{ mg C m}^{-2} \text{ d}^{-1}$  (Table S3), increasing  
68 northwards from the southernmost station up to the PFZ from 32 to  $92 \text{ mg C m}^{-2} \text{ d}^{-1}$ , then decreasing down to  $70 \text{ mg C m}^{-2} \text{ d}^{-1}$   
69 at the SAF. The highest flux was estimated in the SAZ, and the lowest flux was estimated in the STZ.

## 70 4 Discussion

### 71 4.1 Early wintertime $Ba_{\text{xs}}$ and $Ba_{\text{residual}}$ concentrations

72 A noticeable difference between profiles sampled early in the bloom season (Dehairs et al., 1997; Jacquet et al., 2015) versus  
73 those sampled later (Cardinal et al., 2001; Planchon et al., 2013) is the contrasted  $Ba_{\text{xs}}$  concentrations in the surface mixed  
74 layer. Dehairs et al. (1997) has shown that these concentrations of  $Ba_{\text{xs}}$  can be as high as  $9000 \text{ pmol L}^{-1}$  in areas of high  
75 productivity during spring, which then become depleted to concentrations below the SO  $Ba_{\text{residual}}$  value of  $\sim 180 \text{ pmol L}^{-1}$ , as  
76 productivity declines and surface POC export increases (Planchon et al., 2013). These high surface concentrations are,  
77 however, not due to the same process as the one that controls the  $Ba_{\text{xs}}$  concentrations within the mesopelagic zone (Jacquet et  
78 al., 2011). Surface water concentrations are associated with Ba adsorbed onto particles whereas the mesopelagic  $Ba_{\text{xs}}$  signal is  
79 due to barite crystals formed within decaying bio-aggregates (Cardinal et al., 2005; Lam and Bishop, 2007; Lemaitre et al.,  
80 2018; Sternberg et al., 2005). In this study, we observed surface depletion of  $Ba_{\text{xs}}$  at all stations, in line with the assumption  
81 that the bulk surface export from the preceding bloom had been achieved at the time of sampling and, the majority of the  $Ba_{\text{xs}}$   
82 had been transferred to the mesopelagic zone.

83 A sharp increase in  $\sigma_\theta$  observed at the MLD has previously been identified as the depth at which decaying bio-aggregates are  
84 formed (Lam and Bishop, 2007). These increases coincided with an increase in  $Ba_{\text{xs}}$  (Figure 2), linking the subsurface  $Ba_{\text{xs}}$

Deleted: Dehairs et al., 1997

.86 signal to decaying bio-aggregates as per previous studies (Cardinal et al., 2005; Dehairs et al., 1997; Jacquet et al., 2011).  
.87 Additionally, decreases observed in dissolved O<sub>2</sub> profiles along the transect were also accompanied by coinciding increases in  
.88 B<sub>ass</sub>, in line with O<sub>2</sub> consumption due to remineralisation within the mesopelagic zone (Figure 2) (Cardinal et al., 2005; Jacquet  
.89 et al., 2005, 2011). The observed range of mesopelagic B<sub>ass</sub> concentrations (113 - 684 pmol L<sup>-1</sup>) were comparable to those  
.90 previously reported in SO open waters (~ 200 - 1000 pmol L<sup>-1</sup>; Cardinal et al., 2001, 2005; Jacquet et al., 2005, 2008a, 2008b,  
.91 2011, 2015; Planchon et al., 2013).

.92 B<sub>ass</sub> profiles exhibited similar distributions to those reported throughout bloom seasons in the SO, with distinct peaks observed  
.93 within the mesopelagic zone at all stations. Earlier in the bloom season, peaks mostly occur within the upper half of the  
.94 mesopelagic zone (100 - 500 m: Cardinal et al., 2001, 2005; Jacquet et al., 2005, 2008a, 2011, 2015), but as the season  
.95 progresses, they deepen down towards the bottom half of the mesopelagic zone (500 - >1000 m: Jacquet et al., 2008b, Planchon  
.96 et al., 2013). Deepening and widening of the remineralisation depth range can be expected as the season progresses, due to  
.97 continued remineralisation taking place as particles sink to the bottom of the mesopelagic zone (Lemaitre et al., 2018; Planchon  
.98 et al., 2013). This is also what we observed during early winter at stations NPF, with a second peak in deeper waters, as  
.99 observed by Jacquet et al. (2008b) during the iron (Fe) fertilisation experiment (EIFEX). The deeper peak could also be linked  
00 to relatively larger cells that sink faster as they remineralise, possibly a large bloom earlier in the season.

01 A distinct latitudinal trend in mesopelagic depth-weighted average B<sub>ass</sub> has generally been observed in the SO with the highest  
02 values in the PFZ, decreasing north and southwards from the PF. These latitudinal trends tend to be accompanied by a  
03 coinciding trend in in situ surface biomass measurements (Cardinal et al., 2005; Dehairs et al., 1997, Jacquet et al., 2011;  
04 Planchon et al., 2013). During our early winter study, we observed a similar latitudinal trend in mesopelagic B<sub>ass</sub> stock (μmol  
05 m<sup>-2</sup>), with an increase from the southernmost station up to the PF, then varying around a maximum in the SAZ, down to the  
06 lowest value in the STZ, whereas temporally integrated remotely sensed PP increased progressively northwards to a maximum  
07 in the STZ (Figure S1). Time of sampling and extended blooms, which are characteristic of the SAZ (Thomalla et al., 2011),  
08 could be contributing factors to the higher values observed in PP and mesopelagic B<sub>ass</sub> distributions at stations north of the PF  
09 (Figure S1). Contrary to what was expected, the profiles observed during our early winter study still show a significant  
10 mesopelagic remineralisation signal, well after the summer bloom termination, which occurred between April and May (Figure  
11 3), as defined by the point in time when community losses outweigh the growth rate (Thomalla et al., 2011).

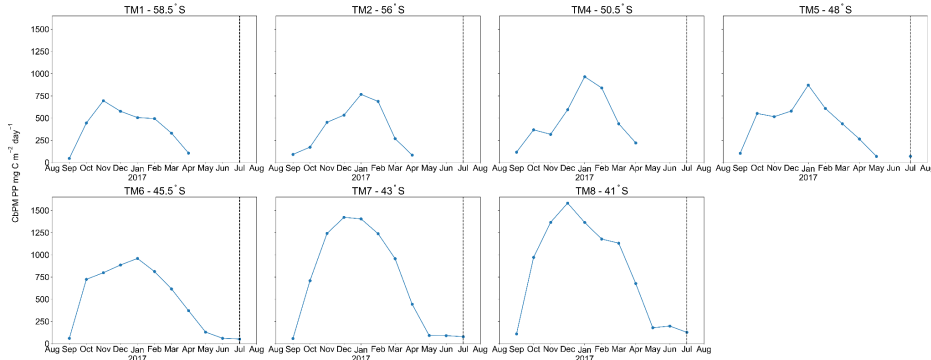


Figure 3: Time series, area-averaged ( $6 \times 1^\circ$  rectangular sample area, positioned  $6^\circ$  upstream longitudinally, and  $1^\circ$  latitudinally centred around each station) remotely sensed CbPM-PP ( $\text{mg C m}^{-2} \text{ day}^{-1}$ ), monthly average from 08/2016 to 08/2017, dashed vertical lines indicate sampling date.

In deeper waters along the transect, south of the STF, (below 2000 m) where remineralisation is minimal compared to the mesopelagic zone, our  $\text{Ba}_{\text{xs}}$  concentration of  $161 \pm 43 \text{ pmol L}^{-1}$  (mean  $\pm$  SD,  $n = 15$ ) is not significantly different from the widely used  $\text{Ba}_{\text{residual}}$  concentration of  $180 \text{ pmol L}^{-1}$ , measured during early Spring to late Summer (e.g., Jacquet et al., 2008a; 2008b; 2011; 2015; Planchon et al., 2013). We thus did not observe a wintertime decline to an expected “true” SO background value, when PP and bacterial activity are suspected to be minimal (Jacquet et al., 2011). There are two possible explanations for this; firstly, the decline to a winter background signal might never be achieved due to ongoing barite precipitation and remineralisation, as well as the release of labile Ba attached to phytoplankton as they decay, precipitating into barite crystals, which could possibly continue throughout winter (Cardinal et al., 2005). Secondly, the low sinking speed of suspended barite ( $\sim 0.3 \text{ m d}^{-1}$ , Sternberg et al., 2008), once produced in the mesopelagic layer, implies that it would take  $\sim 6$  years (not considering reaggregation and redissolution) to sink from 300 m ( $\sim$  peak of production) to the bottom of the mesopelagic layer (1000 m depth). The “true” background value may thus have to be measured at the very end of winter just before the initiation of the spring bloom. This also suggests that the  $\text{Ba}_{\text{xs}}$  signal in the mesopelagic layer may represent remineralisation activity over more than a few days to weeks, per previous reports (e.g., Dehairs et al., 1997; Jacquet et al., 2015; Planchon et al., 2013).

#### 4.2 Timescale of the mesopelagic $\text{Ba}_{\text{xs}}$ signal

The  $\text{Ba}_{\text{xs}}$  signal that we observed in winter is in agreement with the suggestion by Dehairs et al. (1997), that there can be significant carry over between bloom seasons. Other studies have also pointed out that the timescale of this proxy is longer than a snapshot view (Cardinal et al., 2005) and have highlighted a seasonal increase in mesopelagic  $\text{Ba}_{\text{xs}}$  (Jacquet et al., 2011). This strongly suggests that the  $\text{Ba}_{\text{xs}}$  signal is not directly linked to synoptic measurements of PP at the time of sampling. In order to investigate this hypothesis, for the first time, we compiled a SO mesopelagic  $\text{Ba}_{\text{xs}}$  stock dataset with all available

Deleted: Dehairs et al. 1997;

Deleted:

37 literature data including data from this study (Figure 4a, Table S3). The mesopelagic  $B_{\text{As}}$  stock was integrated over the  $B_{\text{As}}$   
38 peak depth range (as identified in each study). As can be seen on the map of the compilation dataset (Figure 4a), these data  
39 points were collected across the three basins of the SO, over ~ 20 years. Despite this diversity in observations, a statistically  
40 significant accumulation of mesopelagic  $B_{\text{As}}$  with time is still observed, SPF (Figures 4b) and NPF (Figures 4c). Mesopelagic  
41  $B_{\text{As}}$  accumulates at a rate of  $0.86 (\pm 0.15) \mu\text{mol m}^{-2} \text{d}^{-1}$  SPF ( $R^2 = 0.43$ , p-value  $< 0.05$ ,  $n = 43$ ; Figure 4b), and at  $0.88 (\pm 0.20)$   
42  $\mu\text{mol m}^{-2} \text{d}^{-1}$  NPF ( $R^2 = 0.41$ , p-value  $< 0.05$ ,  $n = 31$ ; Figure 4c), with no statistically significant difference between the two  
43 regions (Welch's t-test = 0.24; p-value = 0.80).

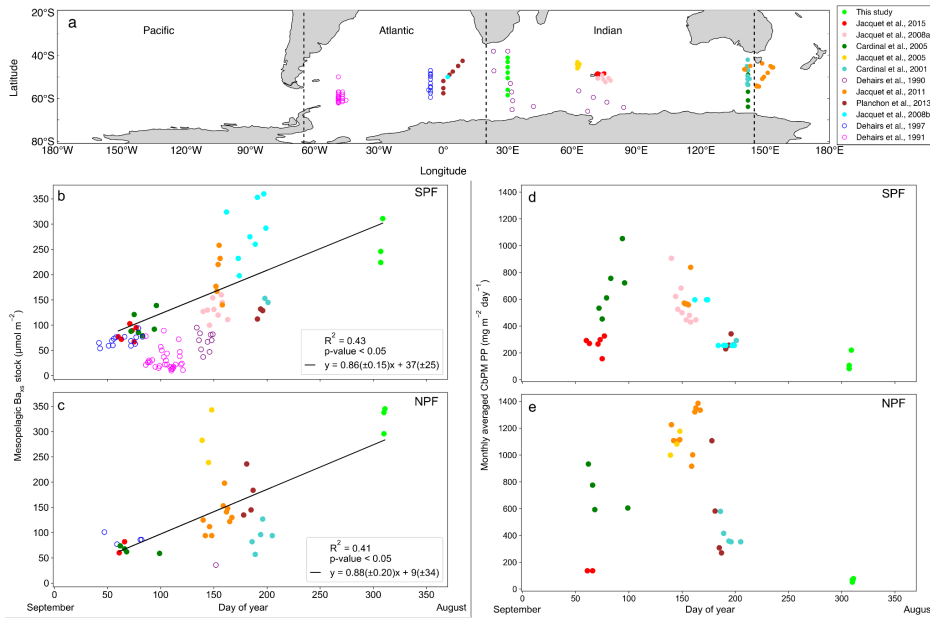
44 A possible link between the integrated mesopelagic  $B_{\text{As}}$  stock and the corresponding integrated remotely sensed PP was  
45 assessed for all studies conducted after September 1997, when remotely sensed PP data became available. To do so, we first  
46 estimated that sub millimetre sized aggregates would take ~ 20 days to sink down to 1000 m (considered as the bottom of the  
47 mesopelagic zone in this study), using a sinking speed of  $50 \text{ m d}^{-1}$ , that corresponds to an average literature value (50 - 100 m  
48  $\text{d}^{-1}$ : Riebesell et al., 1991; 50 - 430  $\text{m d}^{-1}$  around South Georgia: Cavan et al. 2015; mean of ~ 100  $\text{m d}^{-1}$  in the SQ as reviewed  
49 in Laurenceau-Cornec et al., 2015; Marguerite Bay: 10 - 150  $\text{m d}^{-1}$ : McDonnell and Buesseler, 2010). Assuming a maximum  
50 surface current speed of  $0.2 \text{ m s}^{-1}$  (Ferrari and Nikurashin, 2010), it was estimated that these aggregates would have originated,  
51 346 km west from the station that was sampled for mesopelagic  $B_{\text{As}}$ , ~ 20 days prior. Using this distance, the dimensions of  
52 the sample area were set with the southernmost station (TM1) of this study, where degrees of longitude cover the smallest  
53 area. For the sake of consistency this sample area was applied to all sampling locations of the considered dataset. The integrated  
54 remotely sensed PP (see section 2.5) was then averaged spatially, positioned  $6^\circ$  upstream longitudinally, and  $1^\circ$  latitudinally  
55 centred around each station, in order to capture the surface PP that is assumed to translate to the mesopelagic remineralisation  
56 and measured  $B_{\text{As}}$  stock.

57 The monthly averaged remotely sensed PP, at the time of sampling, was compiled for the considered dataset, and we found  
58 that the PP over the growing season (Figure 4d & e) reaches highest values between January and February (day 125 to 175 of  
59 the year), thereafter, steadily decreasing to minimal values in July (~ day 310 of the year, i.e., during our study). The  
60 mesopelagic  $B_{\text{As}}$  accumulation over time can, therefore, not be matched with the remotely sensed PP measured during the  
61 month of sampling. A possible relationship between mesopelagic  $B_{\text{As}}$  stock and temporally integrated remotely sensed PP  
62 was further investigated by considering longer timescales. Remotely sensed PP of the preceding bloom was temporally  
63 integrated from the preceding September, prior to sampling, as the start of the bloom, in general agreement with previous  
64 bloom phenology studies (Thomalla et al., 2011), up to one month prior to the sampling date of the study, taking into  
65 consideration time needed for export, aggregate formation and barite crystal release through remineralisation (~ 1 month).

**Commented [1]:** keep it in full (it has not been asked by the reviewers anyway)

**Commented [2R1]:** I changed this because we have already defined the abbreviation, otherwise it doesn't make sense to use the abbreviation at all

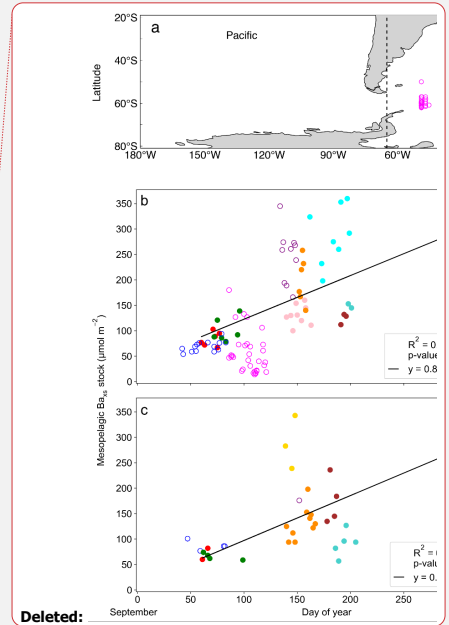
**Deleted:** outhern Ocean



67

68 Figure 4: (a) Positions of  $Ba_{ox}$  observations compiled from all known SO studies, on a cylindrical equal-area projection of the SO, the three SO basin cut offs are indicated by the dashed black lines, from left to right, Pacific, Atlantic and Indian. Integrated mesopelagic  $Ba_{ox}$  stock plotted against day of year sampled, with the 1st of September set as day 1, for all available literature data and winter data from this study. Data was split into two zones using the Polar Front (PF) to divide the SO; (b) South of the PF (SPF) and (c) North of the PF (NPF). Monthly averaged remotely sensed PP plotted against day of year, for locations and dates of the SO compilation dataset and winter data from this study; (d) SPF and (e) NPF. Open circles are data points from studies which did not use HF in the particulate sample digestion procedure, regressions did not include these data, there was, however, no significant difference when including these data points (Table S3).

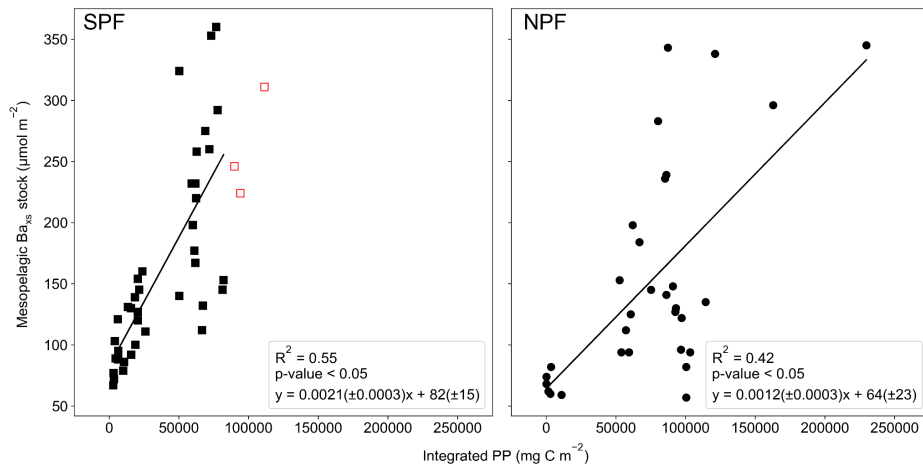
76 Varying timescales were considered between the preceding September up to 1 month prior to sampling (Sept - T1; Table S4), in monthly increments, that could influence the relationship between remotely sensed PP and the mesopelagic  $Ba_{ox}$  stock (Table S4). The strongest and most significant correlation between the mesopelagic  $Ba_{ox}$  stock and integrated remotely sensed PP, for both north and south of the PF, was obtained from the preceding September up to 1 month prior to sampling (Table S4, Sept - T1, SPF: Figure 5a,  $R^2 = 0.55$ ,  $p$ -value < 0.05,  $n = 39$ ; NPF: Figure 5b,  $R^2 = 0.42$ ,  $p$ -value < 0.05,  $n = 31$ ). When remote sensing data was limited due to cloud cover and low sunlight during winter months, specifically at the southernmost stations, all available data was used for the duration of the season. The correlation observed in the STZ is not significant at a 95 % confidence level ( $p$ -value = 0.10); however, the limited number of data points ( $n = 6$ ) may preclude any significance from



Deleted:

85 emerging. The significant positive correlations obtained south of the STF suggest that mesopelagic  $Ba_{xs}$  stock can be used as  
 86 a remineralisation proxy on an annual timescale instead of only a few weeks. Figure 5 also reveals that for a given PP the  
 87 mesopelagic  $Ba_{xs}$  stock was 2-fold higher SPF compared to NPF (Welch's t-test, t-statistic = 2.24; p-value < 0.05), this is  
 88 further discussed below.

89



90

91 **Figure 5: Integrated mesopelagic  $Ba_{xs}$  stock plotted against integrated remotely sensed PP from the preceding September up to one**  
 92 **month prior to sampling, all available literature data and winter data from this study, (a) South of the PF (SPF, black squares) and**  
 93 **(b) North of the PF (NPF, black circles). Red open squares are data points from our winter dataset where there was not sufficient**  
 94 **remote sensing PP data to integrate up to 1 month prior to sampling and available data up to 3 months prior to sampling was plotted**  
 95 **but not included in the statistical analysis.**

96

#### 4.3 Environmental factors influencing mesopelagic remineralisation and carbon export efficiency

97 Estimated POC remineralisation fluxes along the transect ( $6 - 96 \text{ mg C m}^{-2} \text{ d}^{-1}$ ) were on the upper end of the range of fluxes  
 98 reported in previous studies, with the exception of the STZ station, but within the same order of magnitude for the SO as  
 99 estimated from spring to autumn ( $0.2 - 118 \text{ mg C m}^{-2} \text{ d}^{-1}$ ; Table S3; Cardinal et al., 2005; Jacquet et al., 2011, 2015; Planchon  
 00 et al., 2013). As the bloom season progresses, more efficient remineralisation rates have been reported in multiple studies  
 01 (Cardinal et al., 2005; Jacquet et al., 2011; Planchon et al., 2013). However, during late summer as the bloom declines,  
 02 observations indicate an inefficient BCP due to enhanced surface nutrient recycling (Dehairs et al., 1992; Jacquet et al., 2011;  
 03 Planchon et al., 2013), leading to a decrease in surface POC export (Planchon et al., 2013). Seasonal variation is reported to  
 04 be more pronounced northwards within the SO with the least variation observed in the southern Antarctic circumpolar current  
 05 (Dehairs et al., 1997; Planchon et al., 2013).

.06 The percentage of mesopelagic POC remineralisation as calculated from estimated POC remineralisation fluxes over integrated  
.07 remotely sensed PP, for the SO compilation dataset (SPF;  $19 \pm 15\%$ ,  $n = 39$  and NPF;  $10 \pm 10\%$ ,  $n = 29$ ; mean  $\pm$  SD; t-  
.08 statistic = 2.75; p-value  $< 0.05$ ; Table S3), was  $\sim 2$  fold higher SPF than NPF, revealing the higher surface carbon export  
.09 efficiency SPF. Our estimates of % POC remineralised fall within the range of reported export efficiencies throughout the SO  
.10 ( $2 - 58\%$ ; Jacquet et al., 2011; Morris et al., 2007; Savoye et al., 2008). Our values also support the inverse relationship  
.11 between export efficiency and productivity, with higher export efficiency in areas of lower production (High Productivity Low  
.12 E-ratio (HPLE), where E-ratio refers to the ratio between export production and net primary productivity, Fan et al., 2020;  
.13 Maiti et al., 2013). Estimated mesopelagic POC remineralisation has been reported to account for a significant fraction of  
.14 exported carbon in the PFZ and southwards, from 31 to 97 %, from spring to summer, whereas it only accounts for  $\sim 50\%$  in  
.15 the SAZ and SAF, during summer (Cardinal et al., 2005). A combination of variables can influence surface export efficiency  
.16 and the magnitude of the subsequent mesopelagic remineralisation, even more so when considering longer timescales. These  
.17 variables include physical dynamics and interlinked biogeochemical factors, i.e., bacterial activity, phytoplankton community  
.18 structure, zooplankton grazing and nutrient availability (Bopp et al., 2013; Buesseler and Boyd, 2009; Cardinal et al., 2005;  
.19 Jacquet et al., 2008b; Pyle et al., 2018). In previous studies, supply and loss via physical transport has been deemed negligible  
.20 relative to decay and loss via production, due to minimal advection and diffusion gradients observed on the timescale of days  
.21 to weeks. These processes were therefore assumed to have minimal impact on the mesopelagic signal (Dehairs et al., 1997;  
.22 Planchon et al., 2013; Rutgers van der Loeff et al., 2011). It has, however, been observed that features such as mesoscale  
.23 eddies can have an effect on  $B_{as}$  distribution by influencing particle patterns on a broad spatial scale, homogenising  
.24 mesopelagic remineralisation signals by causing relatively flat profiles or shallower remineralisation peaks (Buesseler et al.,  
.25 2005; Jacquet et al., 2008b). The region of our winter study is known for being a mesoscale eddy hotspot due to the South-  
.26 West Indian Ridge (Ansorge et al., 2015). In the STZ, extremely dynamic submesoscale activity due to the Agulhas return  
.27 current may indeed have significantly influenced the mesopelagic signal, and may help explain the absence of correlation with  
.28 integrated surface PP. On the contrary, south of the STF, the significant correlations seem to indicate that physical transport  
.29 variability is not the main process affecting the mesopelagic  $B_{as}$  signal, and that biogeochemical factors may be dominant.  
.30 The Fe-limited SAZ (Ryan-Keogh et al., 2018) and AZ (Viljoen et al., 2018) have generally mixed and seasonally changing  
.31 assemblages of pico-, nano- and micro-phytoplankton (Eriksen et al., 2018; Gall et al., 2001). Diatoms tend to dominate in the  
.32 silicate-rich waters south of the PF (Petrou et al., 2016; Rembauville et al., 2017; Wright et al., 2010), whilst seasonally silicate-  
.33 limited waters north of the PF, favour smaller phytoplankton groups (Freeman et al., 2018; Nissen et al., 2018; Trull et al.,  
.34 2018). HPLE regimes are indeed characteristic of large areas of the SAZ. They are mainly due to surface POC accumulation  
.35 caused by non-sinking particles, tending towards less efficient export of smaller cells (Fan et al., 2020). Even when large  
.36 particles are abundant in HPLE surface layers, a complex grazing community may prevent the export of large particles (Dehairs  
.37 et al., 1992; Lam and Bishop, 2007). This can explain the higher surface carbon export efficiency that we estimate SPF  
.38 compared to NPF. Export efficiency has also been linked to bacterial productivity with efficient surface remineralisation  
.39 limiting surface POC export, when most of the water column integrated bacterial productivity is restricted to the upper mixed

Deleted: HPLE;

Deleted: e

42 layer (Dehairs et al., 1992; Jacquet et al., 2011), which can be the case to varying degrees throughout the SO. In the STZ  
43 phytoplankton communities are reported to be dominated by prokaryotic picoplankton including cyanobacteria and  
44 prochlorophytes (Mendes et al., 2015). These groups utilise regenerated nutrients in the surface mixed layer tending towards  
45 diminished surface export efficiency with high concentrations of non-sinking POC (Fan et al., 2020; Planchon et al. 2013). In  
46 addition to this, the potential influence of high submesoscale activity, may explain the low mesopelagic  $Ba_{xs}$  measured at the  
47 STZ station of this study, despite it being the station with the highest integrated PP (Figure S1). Linking temporally integrated  
48 remotely sensed PP to mesopelagic  $Ba_{xs}$  stock, coupled with the added influence of physical dynamics affecting surface export  
49 efficiencies, along longer timescales, could give better estimates of export and remineralisation signals throughout the SO, on  
50 an annual and basin scale. Our estimates of percentage remineralised POC over remotely sensed PP may contribute to the  
51 improved modelling of the C cycle over the SO, on an annual timescale.

## 52 **5 Conclusions**

53 Our unique early winter  $Ba_{xs}$  data were similar in magnitude and exhibited the same relationship with  $\sigma_\theta$  and dissolved  $O_2$   
54 gradients as observed in summer, indicating that processes controlling this signal in summer are still driving the signal in early  
55 winter. The expected decline of the mesopelagic  $Ba_{xs}$  signal to background values during winter was not observed in this study,  
56 supporting the hypothesis that this remineralisation proxy likely has a longer timescale than previously reported. The absolute  
57 decline might be delayed due to the cumulative behaviour of mesopelagic  $Ba_{xs}$ , ongoing remineralisation and barite  
58 precipitation. The “true” SO background value may thus have to be measured at the very end of winter, prior to bloom initiation.  
59 Significant positive correlations north and south of the PF, between mesopelagic  $Ba_{xs}$  stock and remotely sensed PP, integrated  
60 from September to 1 month before sampling (Sept - T1), in combination with significant  $Ba_{xs}$  accumulation trends obtained  
61 for the SO compilation dataset, suggest an annual timescale. They may also indicate that physical processes do not dominate  
62 the mesopelagic signal on an annual scale, within the SO, and that biogeochemical factors are dominant. There is no significant  
63 difference in mesopelagic  $Ba_{xs}$  and POC remineralisation, north and south of the PF, but the significantly higher integrated  
64 remotely sensed PP to the north when compared to the south, indicates a greater export efficiency south of the PF. This is in  
65 accordance with the phenomenon of HPLE regimes which are common throughout the SO, moreso north of the PF than south  
66 of the PF (Fan et al., 2020). The longer timescale of  $Ba_{xs}$  and the cumulative behaviour of this proxy in the mesopelagic zone  
67 make it possible to use  $Ba_{xs}$  on an annual scale for the estimation of POC remineralisation fluxes throughout the SO and to  
68 better understand how variable environmental factors influence these processes on a basin scale. We believe that the  
69 significance of these relationships will improve as more data become available (e.g., GEOTRACES IDP2021), which will  
70 assist in better understanding and constraining the timescale of remineralisation and C export efficiency throughout the SO.

71 **6 Author contribution**

72 This study was conceptualised by N.R.vH, H.P, G.S and E.B. Formal analysis, investigation and validation of data was carried  
73 out by N.R.vH, H.P, G.S, [E.B](#) and [T.J.R-K](#). [N.R.vH](#) and [T.J.R-K](#) contributed towards the visualisation of the data. H.P, G.S,  
74 T.N.M, A.R, N.L. and E.B contributed towards supervision and resources. Funding was acquired by N.R.vH, T.N.M, A.R and  
75 E.B. All authors contributed towards writing, reviewing, and editing of the final manuscript.

Deleted: and T.N.M

76 **7 Acknowledgments**

77 This work was supported by the ISblue project, Interdisciplinary graduate school for the blue planet (ANR-17-EURE-0015)  
78 and co-funded by a grant from the French government under the program "Investissements d'Avenir". International  
79 collaboration was made possible by funding received by the French-South African National Research Foundation (NRF)  
80 Collaboration (PROTEA; FSTR180418322331), NRF funding (SNA170518231343 and UID 110715) including funding from  
81 South African Department of Science and Technology, French Ministry of National Education, Higher Education and  
82 Research, and the French Ministry of Foreign Affairs and International Development. We would like to thank the captain and  
83 crew of the R/V *SA Agulhas II* for their invaluable efforts, as well as all the research participants who assisted our fieldwork.  
84 Thanks to Prof. I Ansonge, Dr M du Plessis and Dr E Portela for their assistance with water mass identification, and Dr C.  
85 Jeandel for her invaluable expert insight. [Finally, we thank the three reviewers, Prof. F. Dehairs, Dr S. Jacquet, and Prof. J.](#)  
86 [Bishop, for their insightful reviews, thereby improving the quality of our manuscript. A special thank you to Prof. Frank](#)  
87 [Dehairs for sharing the Indigo 3, EPOS 2 and ANTX/6 data.](#)

88 **8 References**

89 Anilkumar, N. and Sabu, P.: Physical process influencing the ecosystem of the indian sector of southern ocean-An overview,  
90 Proc. Indian Natl. Sci. Acad., 83(2), 363–376, doi:10.16943/ptinsa/2017/48960, 2017.  
91 Ansonge, I. J., Jackson, J. M., Reid, K., Durgadoo, J. V., Swart, S. and Eberenz, S.: Evidence of a southward eddy corridor in  
92 the South-West Indian ocean, Deep. Res. Part II Top. Stud. Oceanogr., 119, 69–76, doi:10.1016/j.dsr2.2014.05.012, 2015.  
93 Armstrong, R. A., Peterson, M. L., Lee, C. and Wakeham, S. G.: Settling velocity spectra and the ballast ratio hypothesis,  
94 Deep. Res. Part II Top. Stud. Oceanogr., 56(18), 1470–1478, doi:10.1016/j.dsr2.2008.11.032, 2009.  
95 Barbur, V. A., Montgomery, D. C. and Peck, E. A.: Introduction to Linear Regression Analysis., Stat., 43(2), 339,  
96 doi:10.2307/2348362, 1994.  
97 Behrenfeld, M. J., Boss, E., Siegel, D. A. and Shea, D. M.: Carbon-based ocean productivity and phytoplankton physiology  
98 from space, Global Biogeochem. Cycles, 19(1), 1–14, doi:10.1029/2004GB002299, 2005.  
99 Bishop, J. K. B.: The barite-opal-organic carbon association in oceanic particulate matter, Nature, 332(6162), 341–343,  
00 doi:10.1038/332341a0, 1988.

02 Bishop, J. K. B. and Edmond, J. M.: A new large volume filtration system for the sampling of oceanic particulate matter, *J.*  
03 *Mar. Res.*, 34, 181-198, 1976.

04 Bopp, L., Resplandy, L., Orr, J. C., Doney, S. C., Dunne, J. P., Gehlen, M., Halloran, P., Heinze, C., Ilyina, T., Séférian, R.,  
05 Tjiputra, J. and Vichi, M.: Multiple stressors of ocean ecosystems in the 21st century: Projections with CMIP5 models,  
06 *Biogeosciences*, 10(10), 6225–6245, doi:10.5194/bg-10-6225-2013, 2013.

07 Boyd, P. W., Claustre, H., Levy, M., Siegel, D. A. and Weber, T.: Multi-faceted particle pumps drive carbon sequestration in  
08 the ocean, *Nature*, 568(7752), 327–335, doi:10.1038/s41586-019-1098-2, 2019.

09 Broecker, W. S., Takahashi, T. and Takahashi, T.: Sources and flow patterns of deep-ocean waters as deduced from potential  
10 temperature, salinity, and initial phosphate concentration, *J. Geophys. Res. Ocean.*, 90(C4), 6925–6939,  
11 doi:10.1029/JC090iC04p06925, 1985.

12 Buesseler, K. O.: The decoupling of production and particulate export in the surface ocean, *Global Biogeochem. Cycles*, 12(2),  
13 297–310, doi:10.1029/97GB03366, 1998.

14 Buesseler, K. O., Andrews, J. E., Pike, S. M., Charette, M. A., Goldson, L. E., Brzezinski, M. A. and Lance, V. P.: Particle  
15 export during the Southern Ocean Iron Experiment (SOFeX), *Limnol. Oceanogr.*, 50(1), 311–327,  
16 doi:10.4319/lo.2005.50.1.0311, 2005.

17 Buesseler, K. O. and Boyd, P. W.: Shedding light on processes that control particle export and flux attenuation in the twilight  
18 zone of the open ocean, *Limnol. Oceanogr.*, 54(4), 1210–1232, doi:10.4319/lo.2009.54.4.1210, 2009.

19 Cardinal, D., Dehairs, F., Cattaldo, T. and André, L.: Geochemistry of suspended particles in the Subantarctic and Polar  
20 Frontal zones south of Australia: Constraints on export and advection processes, *J. Geophys. Res. Ocean.*, 106(C12),  
21 31637–31656, doi:10.1029/2000JC000251, 2001.

22 Cardinal, D., Savoye, N., Trull, T. W., André, L., Kopczynska, E. E. and Dehairs, F.: Variations of carbon remineralisation in  
23 the Southern Ocean illustrated by the Baxs proxy, *Deep. Res. Part I Oceanogr. Res. Pap.*, 52(2), 355–370,  
24 doi:10.1016/j.dsr.2004.10.002, 2005.

25 Cavan, E. L., Le Moigne, F. A. C., Poulton, A. J., Tarling, G. A., Ward, P., Daniels, C. J., Fragoso, G. M. and Sanders, R. J.:  
26 Attenuation of particulate organic carbon flux in the Scotia Sea, Southern Ocean, is controlled by zooplankton fecal pellets,  
27 *Geophys. Res. Lett.*, 42(3), 821–830, doi:10.1002/2014GL062744, 2015.

28 Cutter, G., Casciotti, K., Croot, P., Geibert, W., Heimbürger, L.-E., Lohan, M., Planquette, H. and van de Fliedert, T.: Sampling  
29 and Sample-handling Protocols for GEOTRACES Cruises. Version 3, 139pp. & Appendices [online] Available from:  
30 <http://www.geotraces.org/images/stories/documents/intercalibration/Cookbook.pdf>, 2017.

31 de Boyer Montégut, C., Madec, G., Fischer, A. S., Lazar, A. and Iudicone, D.: Mixed layer depth over the global ocean: An  
32 examination of profile data and a profile-based climatology, *J. Geophys. Res. C Ocean.*, 109(12), 1–20,  
33 doi:10.1029/2004JC002378, 2004.

34 Dehairs, F., Baeyens, W. and Goeyens, L.: Accumulation of Suspended Barite at Mesopelagic Depths and Export Production  
35 in the Southern Ocean, *Science (80-.)*, 258(5086), 1332–1335, doi:10.1126/SCIENCE.258.5086.1332, 1992.

36 Dehairs, F., Chesselet, R. and Jedwab, J.: Discrete suspended particles of barite and the barium cycle in the open ocean, *Earth*  
37 *Planet. Sci. Lett.*, 49(2), 528–550, doi:10.1016/0012-821X(80)90094-1, 1980.

38 [Dehairs, F. and Goeyens, L.: Oxidation rate of organic carbon in the mesopelagic water column as traced by suspended barium-](#)  
39 [barite. \*Integr. Mar. Syst. Anal.\*, 205–217, 1996.](#)

40 Dehairs, F., Goeyens, L., Stroobants, N., Bernard, P., Goyet, C., Poisson, A. and Chesselet, R.: On suspended barite and the  
41 oxygen minimum in the Southern Ocean, *Global Biogeochem. Cycles*, 4(1), 85–102, doi:10.1029/GB0041001P00085,  
42 1990.

43 Dehairs, F., Shopova, D., Ober, S., Veth, C. and Goeyens, L.: Particulate barium stocks and oxygen consumption in the  
44 Southern Ocean mesopelagic water column during spring and early summer: Relationship with export production, *Deep*  
45 *Res. Part II Top. Stud. Oceanogr.*, 44(1–2), 497–516, doi:10.1016/S0967-0645(96)00072-0, 1997.

46 Dehairs, F., Stroobants, N. and Goeyens, L.: Suspended barite as a tracer of biological activity in the Southern Ocean, *Mar.*  
47 *Chem.*, 35(1–4), 399–410, doi:10.1016/S0304-4203(09)90032-9, 1991.

48 de Jong, E., Vichi, M., Mehlmann, C. B., Eayrs, C., De Kock, W., Moldenhauer, M. and Audh, R. R.: Sea Ice conditions within  
49 the Antarctic Marginal Ice Zone in winter 2017, onboard the SA Agulhas II., Univ. Cape Town, PANGAEA,  
50 doi:<https://doi.org/10.1594/PANGAEA.885211>, 2018.

51 DeVries, T. and Weber, T.: The export and fate of organic matter in the ocean: New constraints from combining satellite and  
52 oceanographic tracer observations, *Global Biogeochem. Cycles*, 31(3), 535–555, doi:10.1002/2016GB005551, 2017.

53 Ducklow, H. W., Steinberg, D. K. and Buesseler, K. O.: Upper ocean carbon export and the biological pump, *Oceanography*,  
54 14(SPL.ISS. 4), 50–58, doi:10.5670/oceanog.2001.06, 2001.

55 Dymond, J., Suess, E. and Lyle, M.: Barium in Deep-Sea Sediment: A Geochemical Proxy for Paleoproductivity,  
56 *Paleoceanography*, 7(2), 163–181, doi:10.1029/92PA00181, 1992.

57 Ehrhardt, M. (Manfred), Grasshoff, K., Kremling, K. (Klaus) and Almgren, T., Eds.: *Methods of seawater analysis* / edited by  
58 K. Grasshoff, M. Ehrhardt, K. Kremling; with contributions by T. Almgren ... [ et al.], Verlag Chemie, Weinheim., 1983.

59 Eriksen, R., Trull, T. W., Davies, D., Jansen, P., Davidson, A. T., Westwood, K. and Van Den Enden, R.: Seasonal succession  
60 of phytoplankton community structure from autonomous sampling at the Australian Southern Ocean Time Series (SOTS)  
61 observatory, *Mar. Ecol. Prog. Ser.*, 589, 13–21, doi:10.3354/meps12420, 2018.

62 Fan, G., Han, Z., Ma, W., Chen, S., Chai, F., Mazloff, M. R., Pan, J. and Zhang, H.: Southern Ocean carbon export efficiency  
63 in relation to temperature and primary productivity, *Sci. Rep.*, 10(1), 1–11, doi:10.1038/s41598-020-70417-z, 2020.

64 Ferrari, R. and Nikurashin, M.: Suppression of eddy diffusivity across jets in the Southern Ocean, *J. Phys. Oceanogr.*, 40(7),  
65 1501–1519, doi:10.1175/2010JPO4278.1, 2010.

66 Freeman, N. M., Lovenduski, N. S., Munro, D. R., Krumhardt, K. M., Lindsay, K., Long, M. C. and MacLennan, M.: The  
67 Variable and Changing Southern Ocean Silicate Front: Insights from the CESM Large Ensemble, *Global Biogeochem.*  
68 *Cycles*, 32(5), 752–768, doi:10.1029/2017GB005816, 2018.

69 Friedlingstein, P., Jones, M. W., O'Sullivan, M., Andrew, R. M., Hauck, J., Peters, G. P., Peters, W., Pongratz, J., Sitch, S.,  
70 Le Quéré, C., Bakker, D. C. E., Canadell, J. G., Ciais, P., Jackson, R. B., Anthoni, P., Barbero, L., Bastos, A., Bastrikov,  
71 V., Becker, M., Bopp, L., Buitenhuis, E., Chandra, N., Chevallier, F., Chini, L. P., Currie, K. I., Feely, R. A., Gehlen, M.,  
72 Gilfillan, D., Gkritzalis, T., Goll, D. S., Gruber, N., Gutekunst, S., Harris, I., Haverd, V., Houghton, R. A., Hurtt, G., Ilyina,  
73 T., Jain, A. K., Joetzier, E., Kaplan, J. O., Kato, E., Klein Goldewijk, K., Korsbakken, J. I., Landschützer, P., Lauvset, S.  
74 K., Lefèvre, N., Lenton, A., Lienert, S., Lombardozi, D., Marland, G., McGuire, P. C., Melton, J. R., Metzl, N., Munro,  
75 D. R., Nabel, J. E. M. S., Nakaoka, S.-I., Neill, C., Omar, A. M., Ono, T., Peregón, A., Pierrot, D., Poulter, B., Rehder, G.,  
76 Resplandy, L., Robertson, E., Rödenbeck, C., Séférian, R., Schwinger, J., Smith, N., Tans, P. P., Tian, H., Tilbrook, B.,  
77 Tubiello, F. N., van der Werf, G. R., Wiltshire, A. J. and Zaehle, S.: Global Carbon Budget 2019, *Earth Syst. Sci. Data*,  
78 11(4), 1783–1838, doi:10.5194/essd-11-1783-2019, 2019.

79 Gall, M. P., Boyd, P. W., Hall, J., Safi, K. A. and Chang, H.: Phytoplankton processes. Part 1: Community structure during  
80 the Southern Ocean Iron RElease Experiment (SOIREE), *Deep. Res. Part II Top. Stud. Oceanogr.*, 48(11–12), 2551–2570,  
81 doi:10.1016/S0967-0645(01)00008-X, 2001.

82 GEOTRACES Intermediate Data Product Group: The GEOTRACES Intermediate Data Product 2021 (IDP2021), NERC EDS  
83 British Oceanographic Data Centre NOC, doi: 10.5285/cf2d9ba9-d51d-3b7c-e053-8486abc0f5fd, 2021.

84 Gill, A. E.: *Atmosphere-ocean dynamics*, NEW YORK, U.S.A., ACADEMIC PRESS INC., 1982.

85 Gregor, L., Lebehoh, A. D., Kok, S. and Scheel Monteiro, P. M.: A comparative assessment of the uncertainties of global  
86 surface ocean CO<sub>2</sub> estimates using a machine-learning ensemble (CSIR-ML6 version 2019a)-Have we hit the wall?,  
87 *Geosci. Model Dev.*, 12(12), 5113–5136, doi:10.5194/gmd-12-5113-2019, 2019.

88 Gruber, N., Landschützer, P. and Lovenduski, N. S.: The variable southern ocean carbon sink, *Ann. Rev. Mar. Sci.*,  
89 11(September), 159–186, doi:10.1146/annurev-marine-121916-063407, 2019.

90 Honjo, S., Eglinton, T. I., Taylor, C. D., Ulmer, K. M., Sievert, S. M., Bracher, A., German, C. R., Edgcomb, V., Francois, R.,  
91 Deboraglesias-Rodriguez, M., Van Mooy, B. and Repeta, D. J.: Understanding the role of the biological pump in the global  
92 carbon cycle: An imperative for ocean science, *Oceanography*, 27(3), 10–16, doi:10.5670/oceanog.2014.78, 2014.

93 Ito, T., Follows, M. J. and Boyle, E. A.: Is AOU a good measure of respiration in the oceans?, *Geophys. Res. Lett.*, 31(17), 1–  
94 4, doi:10.1029/2004GL020900, 2004.

95 Jacquet, S. H. M., Dehairs, F., Cardinal, D., Navez, J. and Delille, B.: Barium distribution across the Southern Ocean frontal  
96 system in the Crozet-Kerguelen Basin, *Mar. Chem.*, 95(3–4), 149–162, doi:10.1016/j.marchem.2004.09.002, 2005.

97 Jacquet, S. H. M., Dehairs, F., Dumont, I., Becquevort, S., Cavagna, A. J. and Cardinal, D.: Twilight zone organic carbon  
98 remineralization in the Polar Front Zone and Subantarctic Zone south of Tasmania, *Deep. Res. Part II Top. Stud. Oceanogr.*,  
99 58(21–22), 2222–2234, doi:10.1016/j.dsr2.2011.05.029, 2011.

00 Jacquet, S. H. M., Dehairs, F., Elskens, M., Savoye, N. and Cardinal, D.: Barium cycling along WOCE SR3 line in the Southern  
01 Ocean, *Mar. Chem.*, 106(1–2 SPEC. ISS.), 33–45, doi:10.1016/j.marchem.2006.06.007, 2007.

02 Jacquet, S. H. M., Dehairs, F., Lefèvre, D., Cavagna, A. J., Planchon, F., Christaki, U., Monin, L., André, L., Closset, I. and  
03 Cardinal, D.: Early spring mesopelagic carbon remineralization and transfer efficiency in the naturally iron-fertilized  
04 Kerguelen area, *Biogeosciences*, 12(6), 1713–1731, doi:10.5194/bg-12-1713-2015, 2015.

05 Jacquet, S. H. M., Dehairs, F., Savoye, N., Obernosterer, I., Christaki, U., Monnin, C. and Cardinal, D.: Mesopelagic organic  
06 carbon remineralization in the Kerguelen Plateau region tracked by biogenic particulate Ba, *Deep. Res. Part II Top. Stud.*  
07 *Oceanogr.*, 55(5–7), 868–879, doi:10.1016/j.dsr2.2007.12.038, 2008a.

08 Jacquet, S. H. M., Savoye, N., Dehairs, F., Strass, V. H. and Cardinal, D.: Mesopelagic carbon remineralization during the  
09 European Iron Fertilization Experiment, *Global Biogeochem. Cycles*, 22(1), 1–9, doi:10.1029/2006GB002902, 2008b.

10 Jochum, K. P., Nohl, U., Herwig, K., Lammel, E., Stoll, B. and Hofmann, A. W.: GeoReM: A new geochemical database for  
11 reference materials and isotopic standards, *Geostand. Geoanalytical Res.*, 29(3), 333–338, doi:10.1111/j.1751-  
12 908x.2005.tb00904.x, 2005.

13 Kokoska, S. and Zwillinger, D.: *CRC Standard Probability and Statistics Tables and Formulae*, Student Edition., 2000.

14 Lam, P. J. and Bishop, J. K. B.: High biomass, low export regimes in the Southern Ocean, *Deep. Res. Part II Top. Stud.*  
15 *Oceanogr.*, 54(5–7), 601–638, doi:10.1016/j.dsr2.2007.01.013, 2007.

16 Laurenceau-Cornec, E. C., Trull, T. W., Davies, D. M., Bray, S. G., Doran, J., Planchon, F., Carlotti, F., Jouandet, M. P.,  
17 Cavagna, A. J., Waite, A. M. and Blain, S.: The relative importance of phytoplankton aggregates and zooplankton fecal  
18 pellets to carbon export: Insights from free-drifting sediment trap deployments in naturally iron-fertilised waters near the  
19 Kerguelen Plateau, *Biogeosciences*, 12(4), 1007–1027, doi:10.5194/BG-12-1007-2015, 2015.

20 Le Moigne, F. A. C.: Pathways of Organic Carbon Downward Transport by the Oceanic Biological Carbon Pump, *Front. Mar.*  
21 *Sci.*, 6, doi:10.3389/fmars.2019.00634, 2019.

22 Legeleux, F. and Reyss, J. L.: 228Ra/226Ra activity ratio in oceanic settling particles: Implications regarding the use of barium  
23 as a proxy for paleoproductivity reconstruction, *Deep. Res. Part I Oceanogr. Res. Pap.*, 43(11–12), 1857–1863,  
24 doi:10.1016/S0967-0637(96)00086-6, 1996.

25 Lemaitre, N., Planquette, H., Planchon, F., Sarthou, G., Jacquet, S., García-Ibáñez, M. I., Gourain, A., Cheize, M., Monin, L.,  
26 André, L., Laha, P., Terryn, H. and Dehairs, F.: Particulate barium tracing of significant mesopelagic carbon  
27 remineralisation in the North Atlantic, *Biogeosciences*, 15(8), 2289–2307, doi:10.5194/bg-15-2289-2018, 2018.

28 Maiti, K., Charette, M. A., Buesseler, K. O. and Kahru, M.: An inverse relationship between production and export efficiency  
29 in the Southern Ocean, *Geophys. Res. Lett.*, 40(8), 1557–1561, doi:10.1002/GRL.50219, 2013.

30 Marsay, C. M., Sanders, R. J., Henson, S. A., Pabortsava, K., Achterberg, E. P. and Lampitt, R. S.: Attenuation of sinking  
31 particulate organic carbon flux through the mesopelagic ocean, *Proc. Natl. Acad. Sci. U. S. A.*, 112(4), 1089–1094,  
32 doi:10.1073/pnas.1415311112, 2015.

33 McDonnell, A. M. P. and Buesseler, K. O.: Variability in the average sinking velocity of marine particles, *Limnol. Oceanogr.*,  
34 55(5), 2085–2096, doi:10.4319/LO.2010.55.5.2085, 2010.

35 Mendes, C. R. B., Kerr, R., Tavano, V. M., Cavalheiro, F. A., Garcia, C. A. E., Gauns Dessai, D. R. and Anilkumar, N.: Cross-  
36 front phytoplankton pigments and chemotaxonomic groups in the Indian sector of the Southern Ocean, *Deep. Res. Part II*  
37 *Top. Stud. Oceanogr.*, 118, 221–232, doi:10.1016/j.dsr2.2015.01.003, 2015.

38 Morris, P. J., Sanders, R., Turmewitsch, R. and Thomalla, S.: 234Th-derived particulate organic carbon export from an island-  
39 induced phytoplankton bloom in the Southern Ocean, *Deep Sea Res. Part II Top. Stud. Oceanogr.*, 54(18–20), 2208–2232,  
40 doi:10.1016/J.DSR2.2007.06.002, 2007.

41 Nissen, C., Vogt, M., Münnich, M., Gruber, N. and Haumann, F. A.: Factors controlling coccolithophore biogeography in the  
42 Southern Ocean, *Biogeosciences*, 15(22), 6997–7024, doi:10.5194/bg-15-6997-2018, 2018.

43 Orsi, A. H., Whitworth, T. and Nowlin, W. D.: On the meridional extent and fronts of the Antarctic Circumpolar Current,  
44 *Deep. Res. Part I*, 42(5), 641–673, doi:10.1016/0967-0637(95)00021-W, 1995.

45 Passow, U. and Carlson, C. A.: The biological pump in a high CO<sub>2</sub> world, *Mar. Ecol. Prog. Ser.*, 470(2), 249–271,  
46 doi:10.3354/meps09985, 2012.

47 Petrou, K., Kranz, S. A., Trimborn, S., Hassler, C. S., Ameijeiras, S. B., Sackett, O., Ralph, P. J. and Davidson, A. T.: Southern  
48 Ocean phytoplankton physiology in a changing climate, *J. Plant Physiol.*, 203, 135–150,  
49 doi:https://doi.org/10.1016/j.jplph.2016.05.004, 2016.

50 Planchon, F., Cavagna, A. J., Cardinal, D., André, L. and Dehairs, F.: Late summer particulate organic carbon export and  
51 twilight zone remineralisation in the Atlantic sector of the Southern Ocean, *Biogeosciences*, 10(2), 803–820,  
52 doi:10.5194/bg-10-803-2013, 2013.

53 Planquette, H. and Sherrell, R. M.: Sampling for particulate trace element determination using water sampling bottles:  
54 Methodology and comparison to in situ pumps, *Limnol. Oceanogr. Methods*, 10(5), 367–388,  
55 doi:10.4319/lom.2012.10.367, 2012.

56 Pollard, R. T., Lucas, M. I. and Read, J. F.: Physical controls on biogeochemical zonation in the Southern Ocean, *Deep. Res.*  
57 *Part II Top. Stud. Oceanogr.*, 49(16), 3289–3305, doi:10.1016/S0967-0645(02)00084-X, 2002.

58 Pyle, K. M., Hendry, K. R., Sherrell, R. M., Legge, O., Hind, A. J., Bakker, D., Venables, H. and Meredith, M. P.: Oceanic  
59 fronts control the distribution of dissolved barium in the Southern Ocean, *Mar. Chem.*, 204(July), 95–106,  
60 doi:10.1016/j.marchem.2018.07.002, 2018.

61 Rembauville, M., Briggs, N., Ardyna, M., Uitz, J., Catala, P., Penker' h, C., Poteau, A., Claustre, H. and Blain, S.: Plankton  
62 Assemblage Estimated with BGC-Argo Floats in the Southern Ocean: Implications for Seasonal Successions and Particle  
63 Export, *J. Geophys. Res. Ocean.*, 122(10), 8278–8292, doi:10.1002/2017JC013067, 2017.

64 Riebesell, U.: Particle aggregation during a diatom bloom. II. Biological aspects, *Mar. Ecol. Prog. Ser.*, 69(3), 281–291,  
65 doi:10.3354/meps069281, 1991.

66 Rio, M. H., Guinehut, S. and Lamicol, G.: New CNES-CLS09 global mean dynamic topography computed from the  
67 combination of GRACE data, altimetry, and in situ measurements, *J. Geophys. Res. Ocean.*, 116(7), 1–25,  
68 doi:10.1029/2010JC006505, 2011.

69 Robinson, C., Steinberg, D. K., Anderson, T. R., Aristegui, J., Carlson, C. A., Frost, J. R., Ghiglione, J. F., Hernández-León,  
70 S., Jackson, G. A., Koppelman, R., Quéguiner, B., Ragueneau, O., Rassoulzadegan, F., Robison, B. H., Tamburini, C.,  
71 Tanaka, T., Wishner, K. F. and Zhang, J.: Mesopelagic zone ecology and biogeochemistry - A synthesis, *Deep. Res. Part*  
72 *II Top. Stud. Oceanogr.*, 57(16), 1504–1518, doi:10.1016/j.dsr2.2010.02.018, 2010.

73 Rosengard, S. Z., Lam, P. J., Balch, W. M., Auro, M. E., Pike, S., Drapeau, D. and Bowler, B.: Carbon export and transfer to  
74 depth across the Southern Ocean Great Calcite Belt, *Biogeosciences*, 12(13), 3953–3971, doi:10.5194/bg-12-3953-2015,  
75 2015.

76 Rutgers van der Loeff Michiel, M., Cai, P. H., Stimac, I., Bracher, A., Middag, R., Klunder, M. B. and van Heuven, S. M. A.  
77 C.: <sup>234</sup>Th in surface waters: Distribution of particle export flux across the Antarctic Circumpolar Current and in the  
78 Weddell Sea during the GEOTRACES expedition ZERO and DRAKE, *Deep. Res. Part II Top. Stud. Oceanogr.*, 58(25–  
79 26), 2749–2766, doi:10.1016/j.dsr2.2011.02.004, 2011.

80 Ryan-Keogh, T. J., Thomalla, S. J., Mthali, T. N., Van Horsten, N. R. and Little, H. J.: Seasonal development of iron limitation  
81 in the sub-Antarctic zone, *Biogeosciences*, 15(14), 4647–4660, doi:10.5194/bg-15-4647-2018, 2018.

82 Sarmiento, J., & Gruber, N. *Ocean Biogeochemical Dynamics*, Princeton University Press, Princeton, Oxford  
83 doi:10.2307/j.ctt3fgxqx, 2006.

84 Sathyendranath, S., Brewin, R. J. W., Brockmann, C., Brotas, V., Calton, B., Chuprin, A., Cipollini, P., Couto, A. B., Dingle,  
85 J., Doerffer, R., Donlon, C., Dowell, M., Farman, A., Grant, M., Groom, S., Horseman, A., Jackson, T., Krasemann, H.,  
86 Lavender, S., Martinez-Vicente, V., Mazeran, C., Mélin, F., Moore, T. S., Müller, D., Regner, P., Roy, S., Steele, C. J.,  
87 Steinmetz, F., Swinton, J., Taberner, M., Thompson, A., Valente, A., Zühlke, M., Brando, V. E., Feng, H., Feldman, G.,  
88 Franz, B. A., Frouin, R., Gould, R. W., Hooker, S. B., Kahru, M., Kratzer, S., Mitchell, B. G., Muller-Karger, F. E., Sosik,  
89 H. M., Voss, K. J., Werdell, J. and Platt, T.: An ocean-colour time series for use in climate studies: The experience of the  
90 ocean-colour climate change initiative (OC-CCI), *Sensors (Switzerland)*, 19(19), doi:10.3390/s19194285, 2019.

91 Savoye, N., Trull, T. W., Jacquet, S. H. M., Navez, J. and Dehairs, F.: <sup>234</sup>Th-based export fluxes during a natural iron  
92 fertilization experiment in the Southern Ocean (KEOPS), *Deep Sea Res. Part II Top. Stud. Oceanogr.*, 55(5–7), 841–855,  
93 doi:10.1016/J.DSR2.2007.12.036, 2008.

94 Schlitzer, R.: Carbon export fluxes in the Southern Ocean: Results from inverse modeling and comparison with satellite-based  
95 estimates, *Deep. Res. Part II Top. Stud. Oceanogr.*, 49(9–10), 1623–1644, doi:10.1016/S0967-0645(02)00004-8, 2002.

96 Shopova, D., Dehairs, F. and Baeyens, W.: A simple model of biogeochemical element distribution in the oceanic water  
97 column, *J. Mar. Syst.*, 6(4), 331–344, doi:10.1016/0924-7963(94)00032-7, 1995.

98 Sigman, D. M., Hain, M. P. and Haug, G. H.: The polar ocean and glacial cycles in atmospheric CO<sub>2</sub> concentration, *Nature*,  
99 466(7302), 47–55, doi:10.1038/nature09149, 2010.

00 Sternberg, E., Jeandel, C., Robin, E. and Souhaut, M.: Seasonal cycle of suspended barite in the mediterranean sea, *Geochim.*  
01 *Cosmochim. Acta*, 72(16), 4020–4034, doi:10.1016/J.GCA.2008.05.043, 2008.

'02 Sternberg, E., Tang, D., Ho, T. Y., Jeandel, C. and Morel, F. M. M.: Barium uptake and adsorption in diatoms, *Geochim.*  
'03 *Cosmochim. Acta*, 69(11), 2745–2752, doi:10.1016/j.gca.2004.11.026, 2005.

'04 Swart, S., Speich, S., Ansoerge, I. J. and Lutjeharms, J. R. E.: An altimetry-based gravest empirical mode south of Africa: 1.  
'05 Development and validation, *J. Geophys. Res. Ocean.*, 115(3), 1–19, doi:10.1029/2009JC005299, 2010.

'06 Takahashi, T., Sweeney, C., Hales, B., Chipman, D. W., Goddard, J. G., Newberger, T., Iannuzzi, R. A. and Sutherland, S. C.:  
'07 The changing carbon cycle in the southern ocean, *Oceanography*, 25(3), 26–37, doi:10.5670/oceanog.2012.71, 2012.

'08 Taylor, S. R. and McLennan, S. M.: *The continental crust: Its composition and evolution*, Blackwell Scientific Pub., Palo Alto,  
'09 CA, United States. [online] Available from: <https://www.osti.gov/biblio/6582885>, 1985.

'10 Thomalla, S. J., Fauchereau, N., Swart, S. and Monteiro, P. M. S.: Regional scale characteristics of the seasonal cycle of  
'11 chlorophyll in the Southern Ocean, *Biogeosciences*, 8(10), 2849–2866, doi:10.5194/bg-8-2849-2011, 2011.

'12 Trull, T. W., Passmore, A., Davies, D. M., Smit, T., Berry, K. and Tilbrook, B.: Distribution of planktonic biogenic carbonate  
'13 organisms in the Southern Ocean south of Australia: A baseline for ocean acidification impact assessment, *Biogeosciences*,  
'14 15(1), 31–49, doi:10.5194/bg-15-31-2018, 2018.

'15 Twining, B. S., Nodder, S. D., King, A. L., Hutchins, D. A., LeClerc, G. R., DeBruyn, J. M., Maas, E. W., Vogt, S., Wilhelm,  
'16 S. W. and Boyd, P. W.: Differential remineralization of major and trace elements in sinking diatoms, *Limnol. Oceanogr.*,  
'17 59(3), 689–704, doi:<https://doi.org/10.4319/lo.2014.59.3.0689>, 2014.

'18 van Beek, P., François, R., Conte, M., Reyss, J. L., Souhaut, M. and Charette, M.: 228Ra/226Ra and 226Ra/Ba ratios to track  
'19 barite formation and transport in the water column, *Geochim. Cosmochim. Acta*, 71(1), 71–86,  
'20 doi:10.1016/j.gca.2006.07.041, 2007.

'21 Viljoen, J. J., Philibert, R., Van Horsten, N., Mtshali, T., Roychoudhury, A. N., Thomalla, S. and Fietz, S.: Phytoplankton  
'22 response in growth, photophysiology and community structure to iron and light in the Polar Frontal Zone and Antarctic  
'23 waters, *Deep. Res. Part I Oceanogr. Res. Pap.*, 141(September), 118–129, doi:10.1016/j.dsr.2018.09.006, 2018.

'24 Wright, S. W., van den Enden, R. L., Pearce, I., Davidson, A. T., Scott, F. J. and Westwood, K. J.: Phytoplankton community  
'25 structure and stocks in the Southern Ocean (30–80°E) determined by CHEMTAX analysis of HPLC pigment signatures,  
'26 *Deep. Res. Part II Top. Stud. Oceanogr.*, 57(9–10), 758–778, doi:10.1016/j.dsr2.2009.06.015, 2010.

'27 Zhuang, J.: xESMF: Universal Regridder for GeospatialData, <https://github.com/JiaweiZhuang/xESMF>, 2018.

'28